

A Stability Region Criterion for Flat-footed Bipedal Walking on Deformable Granular Terrain

Xiaobin Xiong¹, Aaron D. Ames², and Daniel I. Goldman³

Abstract—Achieving stable bipedal robotic walking on deformable terrain is an open and challenging problem at the intersection of robotics and physics. Ground deformation introduces underactuation; uncertainty in terrain dynamics further complicates dynamical modeling and control methods. This work provides a stability criterion for flat-footed bipedal locomotion and allows model-based control methods to function on homogeneous deformable granular terrain (e.g. sand and dirt). By characterizing static reaction forces from granular materials, in conjunction with granular resistive force theory (RFT), we model and validate a static stability region for the center of mass (CoM) projection of a biped on a granular surface. We show that this stability region approximates the admissible Zero Moment Point (ZMP) region for walking, rendering common Linear Inverted Pendulum Model (LIPM) methods valid with our foot placement strategy. By interpreting the stability region as the maximum reaction moment of the terrain, we formulate walking as a hybrid dynamical system and utilize the *partial hybrid zero dynamics* (PHZD) based methodology to generate walking gaits. Finally, we experimentally validate both the ZMP and PHZD walking gaits on a planar bipedal robot, showing that the stability region criterion permits stable dynamic walking on homogeneous granular terrain.

I. INTRODUCTION

Legged robots, especially bipedal humanoids, have significant advantages over wheeled machines in locomoting both through natural unpaved terrain and in artificial manmade environments. Despite the broad potential applications of bipedal locomotion, such as working in construction sites and planetary exploration, researchers have mainly focused on generating stable walking and running gaits on rigid flat or uneven terrain [1], [2], in which rigid contact between foot and terrain is assumed. Little is known about robotic bipedal walking on deformable terrains such as sand, gravel, and snow. Well-developed walking schemes such as Zero Moment Point (ZMP) [3] and Hybrid Zero Dynamics (HZD) [4], [5] have been successful in numerous robotic systems, but do not apply once the rigid contact assumption becomes invalid. In our effort to understand and enable bipedal locomotion over deformable substrates, we present a study of bipedal walking on homogeneous granular terrain (see Fig. 1). Granular terrain (e.g. sand and dirt) is common on



Fig. 1. Time-lapse photograph of a planar biped walking on a bed of poppy seeds, an experimental surrogate for granular terrain. The robot walked at 10 cm/s. Photo credit: Rob Felt [9].

Earth and other planets, and can exhibit fluid- and solid-like behavior, making it a representative and challenging substrate for locomotion. We choose poppy seeds as our test granular medium because they have been shown useful in several robophysical locomotion studies (e.g. [6], [7] and [8]).

Unlike fluids, the flow of which is modeled by the Navier-Stokes equations, a general model of granular media is not yet available. A friction-based *resistive force theory* (RFT) introduced in [6] was used in [10] and [11] to model the reaction force of the granular media. It assumes linear superposition of forces on infinitesimal partitions of the body in the ‘frictional fluid’ regime where frictional forces dominate material inertial forces. However, the frictional fluid regime assumes movement and does not account for static reaction forces; i.e., RFT predicts forces only when there is relative movement between the body and the granular terrain. One can think of it as a ‘kinetic’ friction-based model.

This paper posits that terrain reaction forces determine the stability of a biped. To model the reaction forces during the intrusion and stoppage of a robot’s foot, we conduct systematic paused intrusion experiments, which facilitate a static reaction model with a single empirically measured quantity, *overshoot ratio*. This model further rationalizes a static stability region criterion of the stability for an Inverted Pendulum (IVP) on granular terrain. We demonstrate that the stability region is the admissible ZMP region for the Linear Inverted Pendulum Model (LIPM). With an additional foot placement strategy, LIPM methods, e.g. ZMP preview control [3], can be utilized to realize walking on granular terrain. We also formulate a hybrid model of walking and utilize *partial hybrid zero dynamics* (PHZD) [12] optimization to generate stable walking gaits. Both ZMP and PHZD walking gaits are experimentally validated on our planar bipedal robot. The experiment video can be found in [13].

*This work is supported by NSF grant CPS-1544857.

¹Xiaobin Xiong is with School of Mechanical Engineering and Institute for Robotics and Intelligent Machines, Georgia Institute of Technology, Atlanta, GA 30332 xiaobin.xiong@gatech.edu

²Aaron D. Ames is with the Department of Mechanical and Civil Engineering and Control and Dynamical Systems, California Institute of Technology, Pasadena, CA 91125 ames@caltech.edu

³Daniel I. Goldman is with School of Physics and School of Biology, Georgia Institute of Technology, Atlanta, GA 30332 daniel.goldman@physics.gatech.edu

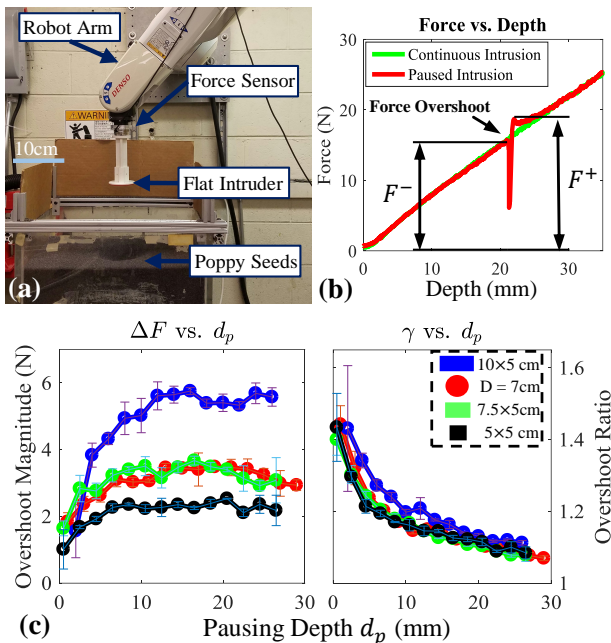


Fig. 2. Paused intrusion experiment to measure static granular intrusion forces. (a) shows the experiment setup. (b) compares the force vs. depth for continuous intrusion and paused intrusion of a 3 cm square intruder. (c) shows force overshoot magnitude ΔF (left) and ratio γ (right) vs. pausing depth for 4 different intruders. The size and shape of each intruder is in the subfigure (right); error bars indicate the standard deviations. For all experiments, pausing time is 3 s. The intrusion speed before and after the pause is 1 cm/s.

II. STATIC STABILITY REGION

In this section, we introduce our granular terrain model, and formulate a stability region criterion for static stability of a biped on granular terrain.

A. Granular Terrain Model

In the context of bipedal walking on granular terrain, the foot-terrain contacts presumably result in kinetic and static interactions. We use RFT [6] to model the resistive forces of continuous interaction. To gain insight into a mechanism which generates static reaction forces, we designed forced vertical intrusion experiment as shown in Fig. 2(a). A force sensor and a flat intruder were attached to the end-effector of the robot arm. The robot arm was commanded to move the intruder vertically into the bed of poppy seeds at a constant speed. Between each experiment, the poppy seeds were initially fluidized with constant air flow from below, which was then turned off for a settling time (~ 30 seconds). The force sensor measured the reaction force from the terrain on the intruder. For a continuous intrusion, the reaction force increased monotonically as in [6]. Initiating a pause during continuous intrusion (*Paused Intrusion*) at a certain depth, i.e. *pausing depth* (d_p), resulted in the reaction force which initially decreased from F^- and then increased beyond the original magnitude to F^+ , as shown in Fig. 2(b). Since the force overshoot occurs at the moment of transition from static to kinetic contact, we model F^+ as the maximum static reaction force. Defining *overshoot magnitude* and *overshoot*

ratio respectively as,

$$\Delta F = F^+ - F^-, \quad (1)$$

$$\gamma = \frac{F^+}{F^-}, \quad (2)$$

we plot ΔF and γ at different d_p for different intruder geometries in Fig. 2(c). For each tested intruder, ΔF increased with d_p near the surface and then saturated at deeper d_p . At a certain d_p , ΔF increased with the intruder size. γ decreased with d_p but was insensitive to intruder size. Therefore, for an arbitrary intruder at a certain d_p , the maximum static reaction force F^+ can be calculated by γF^- . Combining this with RFT [6], we propose a mechanics model of the vertical reaction force as follows:

$$F_z(d_z) = \sigma_z^{\text{RFT}} A, \text{ if } \dot{d}_z > 0, \quad (3)$$

$$F_z(d_z) \leq \gamma \sigma_z^{\text{RFT}} A, \text{ if } \dot{d}_z = 0, \quad (4)$$

where d_z is the intrusion depth, σ_z^{RFT} is the granular stress (N/cm^2) [6], A is the intruder area, and F_z is the vertical reaction force. Note that $\sigma_z^{\text{RFT}} = \alpha d_z$, where α^1 is the constant *unit vertical stiffness* (N/cm^3), i.e. stress per unit depth. One can intuitively understand (3) as a unidirectional spring force condition, since the deformed terrain cannot recover, and interpret (4) as a static friction condition (when the external force is smaller than the maximum static reaction force) that keeps the object stationary.

B. Statics of the Inverted Pendulum Model

A bipedal robot is usually simplified by an Inverted Pendulum (IVP), a low dimensional representation of a biped via a massless pendulum with a point mass attached to the pendulum top. The IVP has proven useful for controlling bipedal walking robots [3]. Here we use this model to analyze the statics of a biped on granular terrain. The ankle joint is at a fixed angle for each configuration. On hard ground, the IVP remains statically upright instead of falling when the Center of Mass (CoM) projection is located inside the foot, i.e. the ‘support polygon.’ On granular terrain, we

¹ $\alpha = \alpha(0, \pi/2)$ in RFT, and 0 and $\pi/2$ are the attack angle and intrusion angle respectively [6].

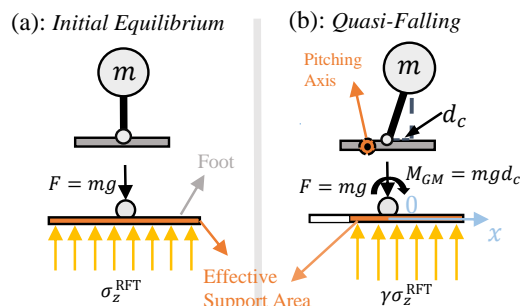


Fig. 3. Static equilibrium of the inverted pendulum on a granular surface in 2D. (a) illustrates the initial equilibrium when the center of mass (CoM) projection exactly locates on the center of the foot. (b) shows the *quasi-falling* situation where the system is about to fall, yet still in equilibrium. The bottom subfigures are the free body diagrams of the foot.

posit that there is also an enclosed region for the CoM projection to keep the IVP statically upright. We define a *quasi-falling* equilibrium as a state in which the projected CoM is on the region boundary and has an infinitesimal translational velocity directed away from the center.

To analyze the *quasi-falling* equilibrium, we first assume the *initial equilibrium*, during which the CoM of the IVP projects onto the foot center as shown in Fig. 3(a). The equilibrium is a result of continuous intrusion, thus

$$mg = \sigma_z^{\text{RFT}} A, \quad (5)$$

where mg is the gravitational force of IVP. The granular reaction force is assumed to be uniformly distributed beneath the foot. The penetration depth is therefore predicted as,

$$d_p = \frac{\sigma_z^{\text{RFT}}}{\alpha} = \frac{mg}{\alpha A}. \quad (6)$$

During *quasi-falling*, the IVP is to fall and pitch about a pitching axis, as shown in Fig. 3(b). A part of the foot penetrates into the terrain and this area is defined as ‘Effective Support Area’ (ESA). We assume that the reaction forces reach the maximum static reaction force in the ESA. Outside of the ESA, where the finite segments of the foot are not penetrating, the reaction forces are zero. We also assume that the reaction force under the ESA is uniform. As the forces and moments are balanced,

$$A_{\text{ESA}} \gamma \sigma_z^{\text{RFT}} = mg, \quad (7)$$

$$\iint_{\text{ESA}} \gamma \sigma_z^{\text{RFT}} x \, dx dy = mg d_c, \quad (8)$$

where d_c is the distance between the CoM projection to the ankle joint. A_{ESA} is the ESA surface area. γ is the force overshoot ratio, which is taken from the empirical paused intrusion data based on the intrusion depth d_p . Equation (7) and (8) provide a solution for d_c . In the planar case that the foot is a line segment, the closed form solution can be found,

$$d_c = \frac{L}{2} \left(1 - \frac{1}{\gamma}\right), \quad (9)$$

where L is the foot length.

C. Stability Region

The *quasi-falling* equilibrium identifies a boundary for static equilibrium of the IVP, i.e. there exists an enclosed ‘Stability Region’ of the CoM projection. If the CoM projection is inside the stability region, $d < d_c$, then the IVP remains stably upright. Otherwise, the terrain yields and the IVP falls. For the planar case in Fig. 3, the stability region is the line segment $[-d_c, d_c]$. Consider a *quasi-falling* equilibrium of the IVP in three dimensions in Fig. 4(a). The assumptions remain the same on the pitching axis and the reaction force beneath ESA. Equation (7) and (8) still hold true. Additionally, the sum of moments about the y axis is balanced,

$$\iint_{\text{ESA}} \gamma \sigma_z^{\text{RFT}} y \, dx dy = 0. \quad (10)$$

Note that the x axis aligns with the line between the ankle and CoM projection; the y axis is perpendicular to the x axis.

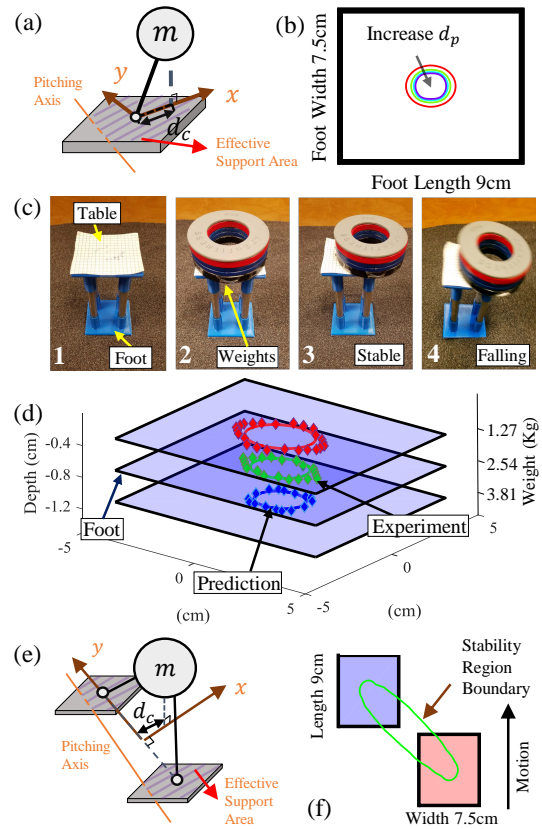


Fig. 4. The stability region of the Inverted Pendulum (IVP). (a) illustrates the ‘quasi-falling’ equilibrium of a general 3D Single Support Phase (SSP). (b) shows the predicted stability region for foot size of 9 cm x 7 cm at depth 6 mm (red), 12 mm (green), 18 mm (cyan) and 24 mm (blue). (c) illustrates the experiment of testing the stability region boundary using the Foot-Table apparatus. (c).2 prepares *initial equilibrium*. (c).3 and (c).4 show that different weight positions yield two different results. (d) overlays the experimental result onto the prediction of the stability region at different depths. (e) illustrates the *quasi-falling* equilibrium with double support. (f) shows the stability region prediction of an IVP of weight 1.4 kg; the red foot is the initial stance foot and blue foot is the nonstance foot. The foot size is 9 cm x 7 cm in all figures.

For a given foot shape and size, (7), (8) and (10) determine the pitching axis and thus d_c . We use a grid method (see Appendix) to discretize the foot into finite elements and numerically calculate d_c for the IVP with a rectangular foot. Fig. 4(b) shows the stability region prediction for the IVP at different depths. For the same foot size, the IVP has a smaller stability region if it more deeply penetrates the terrain. One can conclude that a larger foot leads to less penetration, and therefore provides a larger stability region.

To validate our assumption and mechanics model, we 3D printed a Foot-Table apparatus, shown in Fig. 4(c), to physically represent the IVP. Putting weights at different locations on the table is equivalent to changing the CoM projection of the IVP. A grid paper with 5 mm by 5 mm meshes was glued on the table to measure the weights’ positions. Each experiment followed a procedure of resetting the surface, initial settlement in Fig. 4(c).1 and (c).2 and weight shifting in Fig. 4(c).3 or (c).4. Resetting the surface was done by disturbing the poppy seeds and then sweeping

the surface evenly to create a homogeneously packed state² of the granular terrain. For initial settlement and weight shifting, the weights were moved carefully to reduce impact. Each grid point was tested with multiple experiments. Grid points that resulted in a stable equilibrium represent a stable projection of the CoM. Fig. 4(d) shows the comparison between the experimental results and the numerical calculation of the stability region, from which we conclude that our calculation predicts the stability region well.

The stability criterion of the IVP on hard ground does not necessarily differentiate the Double Support Phase (DSP) from the Single Support Phase (SSP) of a biped, because in DSP two feet becomes a single larger ‘foot’, i.e. the support polygon. However, for DSP on granular terrain, two feet should be considered individually; the contacts of two feet can occur at different depths and have different maximum reaction forces. We consider the *quasi-falling* equilibrium of DSP in Fig. 4(e). The depth difference between two feet is generally small compared to the height of a biped or its CoM, so we assume that the contacts happen on the same horizontal plane (where the pitching axis is in) relative to the robot, but happen at different depths (to calculate reaction force accurately) relative to the terrain surface. With the same assumptions of the existence of the pitching axis and ESA, (7), (8), and (10) hold. Similarly, we use our grid method to calculate the stability boundary. Details are in the Appendix. Fig. 4(f) shows the stability region prediction of DSP.

III. ZERO MOMENT POINT WALKING FORMULATION

A. Admissible ZMP region for dynamic stability

The stability region predicts the static stability of an IVP and indicates the maximum static reaction moment from the granular terrain. For a Linear Inverted Pendulum Model (LIPM) with constant CoM height, the Zero Moment Point (ZMP) position is calculated as [3]:

$$P_{zmp} = \frac{\tau}{mg}, \quad (11)$$

where τ is the ankle torque due to the gravitational force and inertial force of the CoM. The foot remains static and thus the terrain reaction moment balances the ankle torque. The stability region determines the maximum ankle torque and thus the admissible ZMP region,

$$mgd_c = M_{max} = \tau_{max} = mgP_{zmp}. \quad (12)$$

Therefore, the stability region is equivalent to the admissible ZMP region for the LIPM’s dynamics. This is significant because all walking schemes using the LIPM model to satisfy the ZMP criterion can work on bipedal walking on granular terrain by estimating the stability region.

B. ZMP walking synthesis on granular media

We apply the ZMP preview control in [3] to generate walking patterns for a small biped shown in Fig. 5, and ex-

²The volume fraction (compactness of the poppy seeds) was not controlled to be exactly same as that in the intrusion experiments because of the lack of a large fluidized bed for robot walking experiments. However, several paused intrusion experiments on similar manually prepared surface indicate that the overshoot ratios are similar in magnitude.

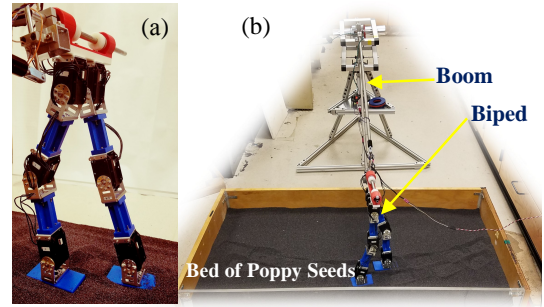


Fig. 5. Robophysical experimental system. (a) The 6 joint bipedal robot (46cm tall, weight 1.4kg). (b) The planar walking experiment setup.

perimentally validate the ZMP admissible region. The ZMP preview control method tracks a ZMP reference trajectory and determines its CoM trajectory for the discretized linear dynamical system of the ZMP equation (see (12) and (13) in [3]). Based on the CoM trajectory and a designed swing foot trajectory, actuation joint trajectories are calculated by inverse kinematics. Then walking can be performed by tracking the joint trajectories.

1) *ZMP reference trajectory*: The reference ZMP trajectory should be designed so that the ZMP lies inside the stability region for all time. An admissible ZMP trajectory for 3D walking is shown in Fig. 6(a). For 2D walking, only the x component of the trajectory is tracked.

2) *Foot placement*: It is important to accommodate vertical foot placement with the terrain deformation. A biped needs to put its swing foot on the terrain surface at the end of the Single Support Phase (SSP) and to shift it down gradually to the estimated depth during the Double Support Phase (DSP). Since in the DSP the CoM moves forward approximately in a linear fashion, the reaction force on the front foot also increases linearly, which requires the front foot to be simultaneously pushed down. Fig. 6(c) illustrates the foot placement strategy. In our implementation, the swing foot trajectories of SSP and DSP are designed separately by cubic splines with zero initial and final velocities. The terrain deformation is estimated by RFT based on the robot weight.

3) *Inverse kinematics*: Because of the small torso, we use the true CoM of the robot instead of the hip joint position to approximate the mass on the linear pendulum. Inverse kinematics is used to calculate each joint angle given the positions of the swing foot and the CoM. We use the Newton-Raphson root-finding method to numerically solve the inverse kinematics problem, usually defined by [14], $x_d - f(\theta_d) = 0$, where θ_d is the vector of desired joint angles. $x_d = [p_{nsf}, p_{CoM}]$ is a vector of the desired positions of the swing foot and the CoM. Thus the Jacobian matrix $\frac{\partial f}{\partial \theta}$ is composed of the swing foot Jacobian and the CoM Jacobian.

4) *Experimental Validation*: We designed the bipedal robot using off-the-shelf servo motors (Robotis, MX-64) and 3D printed parts. The robot was planarized by a counter-weighted boom. Each servo motor is individually controlled by its internal MCU with high PD gains. Joint trajectories

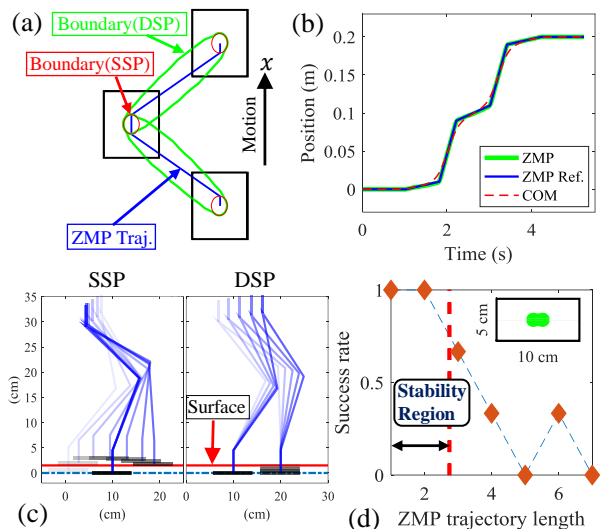


Fig. 6. Zero Moment Point walking on granular terrain. (a) shows one admissible ZMP trajectory (blue) for 3D walking and stability region boundaries in SSP (red) and DSP (green). (b) shows the ZMP and CoM trajectories in the x (forward) direction from preview control given the reference ZMP trajectory in (a). (c) are the stick figures of SSP and DSP to illustrate the foot placement strategy. The penetration depth is exaggerated for illustration purposes. (d) plots the ZMP walking experiment result. The step length is 10 cm and step duration is 2.5 s for all experiments. Subfigure in (d) shows the predicted stability region in the foot.

were computed offline and then loaded onto the servo motors to be executed at 100Hz. As the robot was planarized, we mainly examined the admissible ZMP region in SSP by testing candidate ZMP trajectories. Each candidate ZMP trajectory was designed as a line segment with its center located at the foot center. The lengths of the ZMP line segments varied from 1 cm to 7 cm. Each ZMP trajectory was tested with 3 walking trials. Each walking trial was marked as a success if the biped walked across the poppy seed bed (1.2 m track length), otherwise, it was counted as a failure. Between each experiment, the poppies were prepared similarly to the Foot-Table experiments. As the mass distribution of the robot is not close to the LIPM, the speed of the gaits was designed small (4 cm/s) to reduce dynamic errors from the discrepancy of the mass distribution. The experiment result is plotted in Fig. 6(d), suggesting that the admissible ZMP region is well predicted by the stability region.

IV. HYBRID ZERO DYNAMICS OF WALKING ON GRANULAR TERRAIN

By constraining the dynamics of a biped to that of the linear inverted pendulum, the stability region is the admissible ZMP region for walking. In this section, we interpret the stability region boundary as the maximum terrain reaction moment and incorporate it into *partial hybrid zero dynamics* (PHZD) [5] optimization. Despite the fact that the mechanics understanding of the reaction moment during continuous penetration is missing, experimentally realized walking gaits from optimization are shown to be stable and dynamic.

A. Hybrid System Model

Bipedal walking can be modeled as a periodic multi-domain hybrid control dynamical system with a predetermined ordering of domains, represented by a cyclic directed graph. It is formally defined as a tuple,

$$\mathcal{HC} = (\Gamma, \mathcal{D}, \mathcal{U}, \mathcal{S}, \Delta, FG). \quad (13)$$

Detailed definitions can be found in [5]. A locomotion behavior is mostly described by its domain structure, i.e. the structure of the directed graph, $\Gamma = (V, E)$. For instance, the point foot walking of Mabel [2] can be modeled with a single domain, whereas the human-like walking of AMBER2 [15] is represented by three ordered domains over one step. Proposing a proper domain structure with corresponding guards and constraints is important in configuring the desired walking behavior. In the following, we describe our hybrid model of flat-footed walking on granular terrain.

1) *Domain Structure and Guards*: For walking on granular terrain, we describe a step as three consecutive domains, *Sink*, *Pin*, and *Double Support*, illustrated in Fig. 7(a). *Sink* and *Pin* both are with a single support such that only one foot contacts the terrain. In *Sink*, the stance foot penetrates into the terrain. While in *Pin*, the stance foot stops penetrating and becomes pinned, i.e. having no displacement. When the nonstance foot lands on the terrain, the system switches into *Double Support*. Switching from *Double Support* to *Sink* occurs when the stance foot is about to lift up. All the foot-terrain interactions displace only in the vertical direction. In other words, the foot is not sliding horizontally during contact, which ensures pure vertical foot penetration.

Based on this domain structure, we define the guard condition of $S_{e_s^p}$, i.e. the transition from *Sink* to *Pin*, as $\dot{p}_z = 0, \ddot{p}_z = 0$, that of $S_{e_p^d}$, i.e. the transition from *Pin* to *Double Support*, as $p_z^{nsf} = 0$, and that of $S_{e_d^s}$, i.e. the transition from *Double Support* to *Sink*, as $F_z = 0$, where all terms are illustrated in Fig. 7.

2) *Continuous Dynamics, Holonomic Constraints, and Contact Wrench Constraints*: For each domain \mathcal{D}_v , deriving the equation of motion from the Euler-Lagrange equation [14] yields,

$$D(q)\ddot{q} + H(q, \dot{q}) = Bu + J^T(q)\mathcal{F}, \quad (14)$$

where \mathcal{F} is the vector of contact wrenches, i.e. forces and moments of foot-terrain interactions. J is the Jacobian matrix of the contact positions, defined as,

$$J = \frac{\partial P_c}{\partial q}, \quad (15)$$

where P_c is the vector of contact positions.

For hard ground walking, all contacts introduce *holonomic constraints* as the contacts are rigid, non-penetrable and have no sliding. When the terrain is deformable, a portion of the contacts can be *nonholonomic*. Let P_h denote the *holonomic* contact positions: $P_h \subseteq P_c$, and $P_h \equiv \text{constant}$. Thus, the first and second order differentiations of P_h must be zero:

$$J_h(q)\dot{q} = 0, \quad (16)$$

$$J_h(q)\ddot{q} + \dot{J}_h(q, \dot{q})\dot{q} = 0, \quad (17)$$

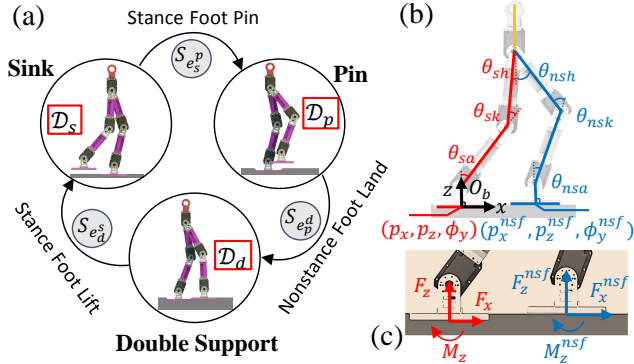


Fig. 7. (a) The directed graph of 3 domain walking on granular terrain. Subscript and superscript s, p, d represent the domains *Sink*, *Pin*, and *Double Support* respectively. (b) The coordinate parameterization. $sa, sk, sh, nsh, nsk, ns_a$ represent the joints of ‘stance ankle’, ‘stance knee’, ‘stance hip’, ‘non-stance hip’, ‘non-stance knee’ and ‘non-stance ankle’ respectively. (c) The reaction forces on the feet.

where $J_h(q) = \frac{\partial P_h}{\partial q}$. Since we enforce vertical flat-foot penetration for all domains, $p_x, \phi_y \in P_h$. In *Pin*, $p_z \in P_h$ as the penetration stops. For *Double Support*, additional holonomic constraints are p_x^{nsf}, ϕ_y^{nsf} .

The contact wrench \mathcal{F} is the reaction from the granular terrain. During continuous penetration, i.e. $\dot{p}_z < 0$, the vertical reaction force is determined by (3). When the penetration stops, i.e. $\dot{p}_z = 0$, the vertical reaction force is limited in magnitude as by (4). We interpolate γ at different depth p_z from experimental data in Fig. 2(c). The lateral force is modeled by Coulomb’s friction model,

$$F_x(p_z) \leq \mu F_z(p_z), \quad (18)$$

where μ is the friction coefficient. We measured it by putting the foot on a tilted plane with a glued layer of poppy seeds. The tilting angle when the foot starts to slip indicates $\mu = 0.466$. We interpret the stability region boundary as the moment constraint about the foot center,

$$M(p_z) \leq M_{\max}(p_z) := mgd_c(p_z). \quad (19)$$

Since the walking is planar, we calculate the stability region boundary d_c from (9). We apply the same force model for the nonstance foot in *Double Support*. The contact wrench constraints in each domain are summarized in Table I.

3) *Discrete Dynamics and Reset Map*: For each guard, there is a reset map Δ to switch the system states of the current domain to the subsequent domain. As the foot-terrain contact is non-rigid for walking on granular deformable terrain, the impact is trivial. For transitions from *Sink* to *Pin* and from *Pin* to *Double Support*, the reset map is an identity matrix. For the transition from *Double Support* to *Sink*, the reset map is the relabeling matrix, as there is a coordinate change.

B. Partial Hybrid Zero Dynamics (PHZD) Optimization

With the hybrid model of walking on granular terrain, we apply the prevalent *PHZD* framework with direct collocation optimization [16] to generate stable walking gaits. [17] and

[15] have shown that with virtual constraints between state variables, the full hybrid dynamics can be projected to a lower dimensional dynamics, i.e. hybrid zero dynamics. Formulating it as an optimization problem is to find local optimal parameters in virtual constraints that result in hybrid invariance while satisfying all the constraints.

1) *Virtual Constraints and Partial Hybrid Zero Dynamics*: Virtual constraints, enforced by feedback control, are defined as parameterized functions that modulate the movement of a robot over a gait cycle [12], [17]. We follow the definition of the virtual constraints in [12], for each domain $v \in \{s, p, d\}$ assuming a constant desired velocity-modulating output $y_{1,v}$ (relative degree $\mathcal{RD} = 1$) and several parameterized position-modulating outputs $y_{2,v}$ ($\mathcal{RD} = 2$),

$$y_{1,v} = \dot{y}_{1,v}^a(q, \dot{q}) - y_{1,v}^d, \quad (20)$$

$$y_{2,v} = y_{2,v}^a(q) - y_{2,v}^d(\alpha_v, \tau(q)), \quad (21)$$

where $y_{1,v}^d = v_d \in \mathbb{R}$ is the desired velocity, and $y_{2,v}^d(\alpha_v, \tau(q))$ is the vector of desired position-modulating outputs. We choose the outputs in Table I and parameterize them by Bézier polynomials [4], the coefficients of which in each domain are represented by α_v . $\tau(q)$ is the state-based parameterization of time, which should monotonically increase over a gait cycle [4]. For the hybrid model of walking on granular terrain, we choose the linearized hip position, $\delta p_{hip}(q) = L_t \theta_{sa} + (L_f + L_t) \theta_{sk}$, to parameterize time and as the velocity-modulating output $y_{1,v}^a(q)$ for all domains [15]. L_t and L_f are the length of tibia and femur link of the robot respectively. With the input/output feedback linearization in [12], the virtual constraints are driven to 0 exponentially by rendering the output dynamics as,

$$\dot{y}_{1,v} = -\epsilon y_{1,v}, \quad (22)$$

$$\ddot{y}_{2,v} = -2\epsilon \dot{y}_{2,v} - \epsilon^2 y_{2,v}. \quad (23)$$

Thus the zero dynamics associated to each domain is invariant. Only enforcing the $\mathcal{RD} = 2$ outputs yields the *partial zero dynamics* surface [12]:

$$\mathcal{PZ}_v = \{(q, \dot{q}) \in \mathcal{D}_v | y_{2,v} = 0, \dot{y}_{2,v} = 0\}, \forall v \in V. \quad (24)$$

If the set of parameters v_d and $\{\alpha_v\}_{v \in V}$ results,

$$\Delta_e(\mathcal{S}_e \cap \mathcal{PZ}_v) \in \mathcal{PZ}_{v+}, \quad (25)$$

for each transition $e \in E$, the manifold $\mathcal{PZ} = \bigcup_{v \in V} \mathcal{PZ}_v$ is *hybrid invariant*. The hybrid control system representing walking has a *partial hybrid zero dynamics* (PHZD) if the control law yields \mathcal{PZ} to be hybrid invariant.

2) *Optimization via Direct Collocation*: Finding proper sets of parameters v_d and $\{\alpha_v\}_{v \in V}$ in the virtual constraints has traditionally been done by solving the PHZD optimization problem [2], [15], defined as,

$$\underset{v_d, \alpha}{\operatorname{argmin}} \quad J(v_d, \alpha), \quad (26)$$

$$\text{s.t.} \quad \Delta_e(\mathcal{S}_e \cap \mathcal{PZ}_v) \in \mathcal{PZ}_{v+}, \quad (27)$$

$$\text{Physical Constraints}, \quad (28)$$

TABLE I
THE HYBRID CONTROL MODEL

Domains	<i>Sink</i>	<i>Pin</i>	<i>Double Support</i>
Contact P_c	$[p_x, p_z, \phi_y]$	$[p_x, p_z, \phi_y]$	$[p_x, p_z, \phi_y, p_x^{nsf}, p_z^{nsf}, \phi_y^{nsf}]$
Holonomic P_h	$[p_x, \phi_y]$	$[p_x, p_z, \phi_y]$	$[p_x, p_z, \phi_y, p_x^{nsf}, \phi_y^{nsf}]$
Guard Condition	$\dot{p}_x = 0, \ddot{p}_x = 0$	$p_z^{nsf} = 0$	$F_z = 0$
Wrench Constraints	$F_z = \alpha A p_z,$ $F_x \leq \mu F_z,$ $M_z \leq M_{\max}(p_z)$	$F_z \leq \gamma(p_z) \alpha A p_z,$ $F_x \leq \mu F_z,$ $M_z \leq M_{\max}(p_z)$	$F_z \leq \gamma(p_z) \alpha A p_z, F_z^{nsf} = \alpha A p_z^{nsf},$ $F_x \leq \mu F_z, F_x^{nsf} \leq \mu F_z^{nsf},$ $M_z \leq M_{\max}(p_z), M_z^{nsf} \leq M_{\max}(p_z^{nsf})$
Reset Map \mathcal{R}	Identity matrix	Identity matrix	Relabeling matrix
$\dot{y}_{1,v}^a(q, \dot{q})$	$\delta \dot{p}_{hip}(q)$	$\delta \dot{p}_{hip}(q)$	$\delta \dot{p}_{hip}(q)$
$y_{2,v}^a(q)$	$[\theta_{sk}, \theta_{Torso}, \theta_{nsh}, \theta_{nsk}, \theta_{nsf}]^4$	$[\theta_{sk}, \theta_{Torso}, \theta_{nsh}, \theta_{nsk}, \theta_{nsf}]$	$[\theta_{sk}, \theta_{Torso}, \theta_{nsh}, \theta_{nsf}]$

where $J(v_d, \alpha)$ is the cost function and (27) is the hybrid invariant constraint. Physical constraints include guard constraints, contact wrench constraints and etc. [16] introduced a generalized framework that utilizes direct collocation optimizing high dimensional dynamical systems through discretization and approximation, to simplify expressions of constraints and generate analytic Jacobian matrices. The result is a fast and reliable method of solving the optimization problem. We apply the same approach to solve the optimization of walking on granular terrain to find the proper virtual constraints. See more details in [16].

$${}^3\theta_{Torso} := \theta_{sa} + \theta_{sk} + \theta_{sh}.$$

$${}^4\theta_{nsf} := -\theta_{sa} - \theta_{sk} - \theta_{sh} + \theta_{nsa} + \theta_{nsk} + \theta_{nsh}.$$

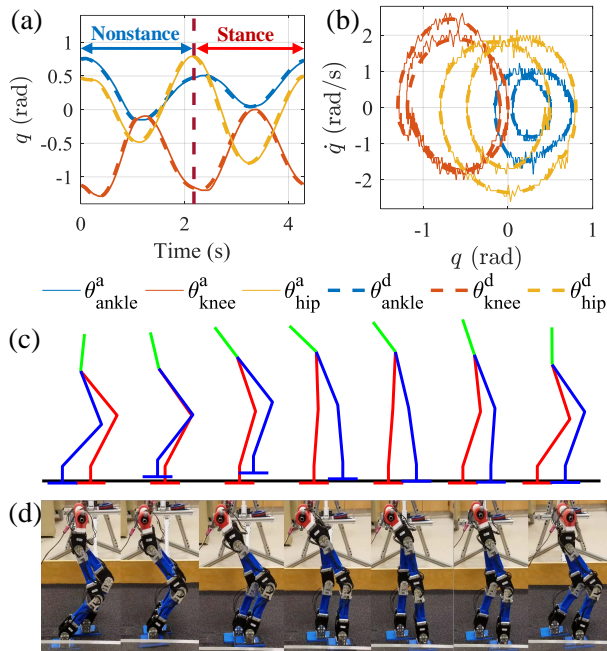


Fig. 8. Implemented walking from *partial hybrid zero dynamics* optimization. (a) Position tracking of the gait on one leg during two steps. (b) The limit cycles of three joints on one leg. In both (a) and (b), dashed lines are simulation results; solid lines are experimental results from the encoder readings. (c) and (d) are the snapshot comparison between simulation and experiment over one step. Time between snapshots is ~ 0.37 s. The torso has trivial inertia and thus is bent backward in *Sink* and *Pin* (when one leg swings forward) to keep its applied ankle torque (equivalent to ground reaction moment) small.

C. Gait Generation and Experimental Results

We chose the mechanical cost of transport as our optimization objective, and configured all constraints for walking on poppy seeds. The formulated optimization problem was solved using IPOPT [18] with linear solver ma57. The solved virtual constraints were evaluated by simulating the full dynamics model of the biped with our terrain model using the MATLAB ode45 integrator. The exponential stability of the periodic orbit is examined by checking that the maximum magnitude of the eigenvalues of the Jacobian of the Poincaré return map is less than one [17]. Numerically evaluation found a maximum eigenvalue magnitude of 0.67, indicating exponential stability. The stable gait with joint trajectories was saved and tracked by joint motors to implement walking with the biped. Fig. 8 shows the simulation and experiment results. The walking is stable, as depicted in Fig. 8(d), even in the presence of small terrain disturbances as shown in the experiment video [13].

V. CONCLUSION AND FUTURE WORK

In this work, we integrated our measurement of granular reaction forces with re-synthesized control schemes (e.g. ZMP preview control and PHZD optimization), which first allowed model-based control methods to yield dynamic bipedal walking on a deformable terrain—dry granular media. Although the underlying physics which generate the static forces have not been identified, the empirically measured overshoot ratios were useful in predicting the stability regions. Stable walking can be achieved on granular terrain by only estimating this region without exhaustive sensing. The resultant walking is still flat-footed, and thus the foot-terrain interaction is conservative due to the moment constraints. Walking on non-flat deformable terrain or terrain with irregularities cannot be handled by our method. In the future, we will study more aggressive foot-terrain contact (e.g. pivoting during interaction), and aim to develop appropriate online learning schemes with closed-loop control to achieve walking on general deformable terrain.

APPENDIX

Numerical calculation of the stability region boundary: The procedure is to find the Effective Support Area (ESA) and pitching axis in the *quasi-falling* equilibrium and then calculate d_c . As the integration is difficult to calculate over a

rectangle area, we discretize the rectangle by small squares and numerically find the number N of squares in ESA. We assume that the pitch axis direction k is within a range of y axis direction, and thus generate a vector K of candidate pitching axis directions. Find the k_i in K which results in the minimum reaction moment M_x about the x axis, and then use this as the pitch axis ϕ_k . Finally, calculate the reaction moment M_y about the y axis and thus d_c . The detailed procedure is given in Algorithm 1.

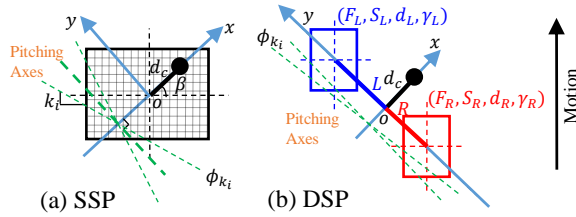


Fig. 9. Calculation illustration. Refer to Fig. 4(a) for SSP and (e) for DSP.

Algorithm 1 Stability Region Boundary for SSP

Input: $mg, \alpha(0, \pi)$

- 1: $\sigma_z^{\text{RFT}}, d_p \leftarrow mg$ from (5) and (6), and $\gamma \leftarrow d_p$
- 2: $A_{\text{ESA}} \leftarrow mg, \gamma, \sigma_z^{\text{RFT}}$ from (7)
- 3: Foot Discretization, $N \leftarrow A_{\text{ESA}}$
- 4: **for each** $\beta \in [0, 2\pi]$ **do**
- 5: Initialize K
- 6: **for each** k_i in K **do**
- 7: Find $\phi_{k_i} \leftarrow N$, and $M_x(k_i) \leftarrow \phi_{k_i}$ from (8)
- 8: **end for**
- 9: $k, \phi_k \leftarrow \operatorname{argmin}_{k_i} M_x(k_i)$, and $M_y \leftarrow k, \phi_k$
- 10: $d_c \leftarrow M_y$ from (10)
- 11: **end for**
- 12: **return** $d_c(\beta)$

We assume that DSP happens after SSP. The swing foot starts at the terrain surface and sinks as the CoM shifts. Assume that right foot was the stance foot during SSP. Thus $(F_L, F_R) = (0, mg)$ initially, where F_L or F_R is the sum of reaction forces beneath the foot in magnitude. The detailed procedure is given in Algorithm 2.

ACKNOWLEDGMENT

We would like to all members in Crablab, especially Jennifer Rieser, Christian Hubicki and Perrin Schiebel for intrusion experiment setup, Jeffrey Aguilar and Allison Kim for initial data collection, and Andras Karsai for careful reading of this paper. We thank Ayonga Hereid for help on optimization implementation.

REFERENCES

- [1] F. Iida and R. Tedrake, “Minimalistic control of biped walking in rough terrain,” *Autonomous Robots*, vol. 28, no. 3, pp. 355–368, 2010.
- [2] J. W. Grizzle, J. Hurst, B. Morris, H.-W. Park, and K. Sreenath, “Mabel, a new robotic bipedal walker and runner,” in *American Control Conference, 2009. ACC’09*. IEEE, 2009, pp. 2030–2036.

Algorithm 2 Stability Region Boundary for DSP

Input: $mg, \alpha(0, \pi)$, Step Length($StepL, StepW$)

- 1: $\sigma_{z_R}^{\text{RFT}}, d_R, \gamma_R \leftarrow$ Algorithm 1
- 2: **for each** $L \in [0, \sqrt{StepL^2 + StepW^2}]$ **do**
- 3: $F_L, F_R \leftarrow F_L + F_R = mg, F_L L + F_R R = 0$
- 4: $\sigma_{z_L}^{\text{RFT}}, d_L, \gamma_L \leftarrow F_L$
- 5: $A_{\text{ESA}}^L, A_{\text{ESA}}^R \leftarrow F_L, F_R, \sigma_{z_L}^{\text{RFT}}, \sigma_{z_R}^{\text{RFT}}, \gamma_L, \gamma_R$
- 6: Foot Discretization, $N_L, N_R \leftarrow A_{\text{ESA}}^L, A_{\text{ESA}}^R$
- 7: Initialize K
- 8: **for Each** k_i in K **do**
- 9: Find $\phi_{k_i} \leftarrow N_R$, and $N_L(k_i) \leftarrow \phi_{k_i}$
- 10: $\Delta N_L(k_i) = |N_L(k_i) - N_L|$
- 11: **end for**
- 12: $k, \phi_k \leftarrow \operatorname{argmin}_{k_i} \Delta N_L(k_i)$, and $M_y \leftarrow \phi_k$
- 13: $d_c \leftarrow M_y$
- 14: **end for**
- 15: **return** $d_c(L)$

- [3] S. Kajita, F. Kanehiro, K. Kaneko, K. Fujiwara, K. Harada, K. Yokoi, and H. Hirukawa, “Biped walking pattern generation by using preview control of zero-moment point,” in *Robotics and Automation, 2003. Proceedings. ICRA’03. IEEE International Conference on*, vol. 2. IEEE, 2003, pp. 1620–1626.
- [4] E. R. Westervelt, J. W. Grizzle, and D. E. Koditschek, “Hybrid zero dynamics of planar biped walkers,” *IEEE transactions on automatic control*, vol. 48, no. 1, pp. 42–56, 2003.
- [5] A. D. Ames, R. Vasudevan, and R. Bajcsy, “Human-data based cost of bipedal robotic walking,” in *Proceedings of the 14th international conference on Hybrid systems: computation and control*. ACM, 2011, pp. 153–162.
- [6] C. Li, T. Zhang, and D. I. Goldman, “A terradynamics of legged locomotion on granular media,” *Science*, vol. 339, no. 6126, pp. 1408–1412, 2013.
- [7] C. M. Hubicki, J. Aguilar, D. I. Goldman, and A. D. Ames, “Tractable terrain-aware motion planning on granular media: An impulsive jumping study,” in *Intelligent Robots and Systems (IROS), 2016 IEEE/RSJ International Conference on*. IEEE, 2016, pp. 3887–3892.
- [8] J. Aguilar and D. I. Goldman, “Robophysical study of jumping dynamics on granular media,” *Nature Physics*, 2015.
- [9] “Georgia tech research horizons, complicated walking,” <http://www.rh.gatech.edu/exhibit-a/complicated-walking>, 2016.
- [10] T. Zhang and D. I. Goldman, “The effectiveness of resistive force theory in granular locomotion,” *Physics of Fluids*, vol. 26, no. 10, p. 101308, 2014.
- [11] R. L. Hatton, Y. Ding, H. Choset, and D. I. Goldman, “Geometric visualization of self-propulsion in a complex medium,” *Physical review letters*, vol. 110, no. 7, p. 078101, 2013.
- [12] A. D. Ames, “Human-inspired control of bipedal walking robots,” *IEEE Transactions on Automatic Control*, vol. 59, no. 5, pp. 1115–1130, 2014.
- [13] <https://youtu.be/7sjJs95awK8>.
- [14] K. M. Lynch and F. C. Park, *Modern Robotics: Mechanics, Planning, and Control*. Cambridge University Press, 2017.
- [15] H. Zhao, A. Hereid, W.-I. Ma, and A. D. Ames, “Multi-contact bipedal robotic locomotion,” *Robotica*, pp. 1–35, 2015.
- [16] A. Hereid, E. A. Cousineau, C. M. Hubicki, and A. D. Ames, “3d dynamic walking with underactuated humanoid robots: A direct collocation framework for optimizing hybrid zero dynamics,” in *Robotics and Automation (ICRA), 2016 IEEE International Conference on*. IEEE, 2016, pp. 1447–1454.
- [17] E. R. Westervelt, J. W. Grizzle, C. Chevallereau, J. H. Choi, and B. Morris, *Feedback control of dynamic bipedal robot locomotion*. CRC press, 2007, vol. 28.
- [18] A. Wächter and L. T. Biegler, “On the implementation of an interior-point filter line-search algorithm for large-scale nonlinear programming,” *Mathematical programming*, vol. 106, no. 1, pp. 25–57, 2006.